

# Nature of bright C-complex asteroids

Sunao HASEGAWA,<sup>1,\*</sup> Toshihiro KASUGA,<sup>2</sup> Fumihiko USUI,<sup>3</sup> and Daisuke KURODA<sup>4</sup>

<sup>1</sup>Institute of Space and Astronautical Science, Japan Aerospace Exploration Agency, 3-1-1 Yoshinodai, Chuo-ku, Sagami-hara 252-5210, Japan

<sup>2</sup>Public Relations Center, National Astronomical Observatory of Japan, 2-21-1 Osawa, Mitaka-shi, Tokyo 181-8588, Japan

<sup>3</sup>Center for Planetary Science, Graduate School of Science, Kobe University, 7-1-48, Minatojima-minamimachi, Chuo-Ku, Kobe 650-0047, Japan

<sup>4</sup>Okayama Astronomical Observatory, Graduate School of Science, Kyoto University, 3037-5 Honjo, Kamogata-cho, Asakuchi, Okayama 719-0232, Japan

\*E-mail: hasehase@isas.jaxa.jp

Received ; Accepted

## Abstract

Most C-complex asteroids have albedo values less than 0.1, but there are some high-albedo (bright) C-complex asteroids with albedo values exceeding 0.1. To reveal the nature and origin of bright C-complex asteroids, we conducted spectroscopic observations of the asteroids in visible and near-infrared wavelength regions. As a result, the bright B-, C-, and Ch-type (Bus) asteroids, which are subclasses of the Bus C-complex, are classified as DeMeo C-type asteroids with concave curvature, B-, Xn-, and K-type asteroids. Analogue meteorites and material (CV/CK chondrites, enstatite chondrites/achondrites, and salts) associated with these spectral types of asteroids are thought to be composed of minerals and material exposed to high temperatures. A comparison of the results obtained in this study with the SDSS photometric data suggests that salts may have occurred in the parent bodies of 24 Themis and 10 Hygiea, as well as 2 Pallas. The bright C-complex asteroids in other C-complex families were likely caused by impact heating. Bright C-complex asteroids that do not belong to any families are likely to be impact metamorphosed carbonaceous chondrites, CV/CK chondrites, or enstatite chondrites/achondrites.

**Key words:** methods: observational — minor planets, asteroids: general — techniques:spectroscopic

## 1 Introduction

In the 1970s, within several years after the first spectrophotometric study of asteroids (McCord, Adams, & Johnson 1970), asteroids with flat reflectance spectra over the visible wavelength range were discovered (Johnson & Fanale 1973; McCord & Gaffey 1974; Chapman, Morrison, & Zellner 1975). Since these asteroids have spectral and physical properties similar to carbonaceous chondrites (e.g., Johnson & Fanale 1973; McCord & Gaffey 1974; Chapman, Morrison, & Zellner 1975) and interplanetary dust particles (e.g., Vernazza et al. 2015;

Hasegawa et al. 2017), the asteroids are considered as parent bodies of these chondrites. These asteroids with flat reflectance spectra over the visible wavelength range are defined or categorized as C-complex/group/type asteroids (hereafter C-complex asteroids) (Chapman, Morrison, & Zellner 1975; Tholen 1984; Bus & Binzel 2002b). The albedo of C-complex asteroids is typically below 0.1 (Chapman, Morrison, & Zellner 1975; Tedesco et al. 1989). The major trends in the distribution of the albedo of C-complex asteroids have not shown significant differences in recent studies that used infrared astronomical

satellites dedicated to all-sky surveys, AKARI (Murakami et al. 2007) and WISE (Wright et al. 2010); however, small C-complex asteroids with albedos greater than 0.1 were found (Mainzer et al. 2011b, 2012; Usui et al. 2013).

To examine characteristics of C-complex asteroids with the geometric albedo of more than 0.1 (hereafter “bright” C-complex asteroids) in more detail, Kasuga et al. (2013, 2015) conducted near-infrared spectroscopic observations of bright C-complex asteroids in the outer main-belt and no signs of water ice were found in the bright C-complex asteroids. These studies argue that Mg-rich amorphous and/or crystalline silicates on the surface of the asteroids can be responsible for the high-albedo values. The presence of crystalline silicate implies the occurrence of high-temperature environments during planetesimal formation, which was confirmed in some of the observed bright C-complex asteroids.

It is essential to classify the reflectance spectra of asteroids in order for knowing the properties of the surface materials on asteroids. The Bus taxonomy (Bus & Binzel 2002b) that classifies asteroids using visible reflectance spectra according to principal component analysis (PCA) and the Bus–DeMeo taxonomy (DeMeo et al. 2009; Binzel et al. 2019) does those using the visible and near-infrared spectra according to PCA are the most popular and important classification methods for classifying asteroids. In particular, the Bus–DeMeo taxonomy is based on spectra with more wide wavelength range, so it is expected that more detailed asteroid properties will be extracted.

In this study, we made spectroscopic observations in visible and near-infrared wavelength regions, to obtain the reflectance spectra of the bright C-complex asteroids. On the basis of obtained near-infrared spectroscopic results of bright C-complex asteroids, we discuss the origin of the bright C-complex asteroids using large amounts of the spectrophotometric data of asteroids. The subsequent sections of this paper describe the observations and data reduction procedures (section 2), presents the spectroscopic and taxonomic results of bright C-complex asteroids (section 3) and the boundaries of albedoes for bright C-complex asteroids (section 4), and discusses the nature and origin of the asteroids (section 5).

## 2 Observations and data reduction procedures

In order to carry out the Bus–DeMeo taxonomy of bright C-complex asteroids for which visible spectra have already been known in the literatures, near-infrared spectroscopic observations for the asteroids were performed in this study. Main candidates for observations in near-infrared wavelength regions were assigned bright C-complex asteroids on the basis of the Bus taxonomy (Bus & Binzel 2002b; Lazzaro et al. 2004)<sup>1</sup> listed in the AKARI asteroid catalogs (Usui et al. 2011; Hasegawa

et al. 2013). A bright T-type asteroid, which typically has low albedo characteristics, was also observed (979 Ilsewa). Besides, to increase the sample of bright C-complex asteroids, visible spectroscopic observations for bright “unknown-type” asteroids were carried out. Unknown spectral type candidates were selected from bright asteroids in the outer main-belt region, where many C-complex asteroids are distributed, listed in the AKARI asteroid catalogs. Furthermore, spectroscopic observations of several “known as” C-complex asteroids with low albedo, which are located in the outer main-belt region, were also conducted to evaluate the reliability of the obtained reflectance spectra.

The spectroscopic observations for bright C-complex asteroids were conducted at two observatories: the Subaru Telescope, National Astronomical Observatory of Japan (NAOJ), National Institute of Natural Sciences (NINS) on Mt. Mauna Kea in Hawaii, USA (Minor Planet Center (MPC) code: 568) from 2012 February to 2013 April; the Okayama Astrophysical Observatory, NAOJ, NINS, in Okayama, Japan (MPC code 371) during December 2013 and January 2014. Ten and eleven spectroscopic observations of the asteroids were made with the Subaru telescope and Okayama Astrophysical Observatory, respectively. The nightly observational details for the spectroscopy are listed in table 1.

<sup>1</sup> Taxonomic data in Carvano et al. (2010) were not available when selecting the candidates in this study.

**Table 1.** Spectroscopic circumstances of the asteroids.

Num	Name	Date (UT) [YY.MM.DD]	Start–End time [hr:min]	$R_h^*$ [au]	$\Delta^*$ [au]	$\alpha^*$ [°]	Airmass	Instr.	Solar analogue
320	Katharina	2013.01.06	08:54–09:49	2.927	1.994	7.4	1.01–1.02	IRCS	HD283798
366	Vincentina	2012.11.25	06:21–07:17	3.044	2.573	17.8	1.08–1.17	IRCS	SA115-271
419	Aurelia	2012.02.17	12:01–12:25	2.709	1.761	7.3	1.07–1.08	IRCS	SA103-272, HIP52192
840	Zenobia	2012.11.25	12:53–14:16	3.433	2.915	15.2	1.02–1.13	IRCS	HD79078, SA98-978
979	Ilsewa	2012.11.25	04:55–05:58	2.736	2.626	23.2	1.12–1.25	IRCS	SA115-271
981	Martina	2012.02.17	08:13–09:22	3.496	2.633	9.1	1.00–1.03	IRCS	SA97-249, LTT12162
1301	Yvonne	2013.04.06	12:46–15:23	3.189	2.674	16.9	1.01–1.12	IRCS	SA102-1081
1764	Cogshall	2013.12.06	14:02–16:03	3.462	2.494	3.6	1.05–1.12	KOOLS	HD28099, HD89010
2250	Stalingrad	2013.12.05	10:34–11:26	2.814	2.169	17.3	1.16–1.19	KOOLS	HD1368
2310	Olshaniya	2013.12.06	09:25–10:44	2.934	2.459	18.5	1.23–1.24	KOOLS	HD1368, SA93-101, SA98-978, SA102-1081
2376	Martynov	2013.12.08	17:02–18:38	3.263	2.468	11.8	1.02–1.05	KOOLS	HD25680, HD65523, HD70088
2519	Annagerman	2012.02.16	11:45–12:13	3.466	2.644	10.4	1.09–1.13	IRCS	SA103-272, HD127913
2525	O'Steen	2012.02.16	12:47–13:28	3.725	3.122	13.2	1.16–1.23	IRCS	SA103-272, WASP-1
2667	Oikawa	2013.12.06	12:03–12:49	2.735	1.955	15.0	1.10–1.11	KOOLS	HD28099, HD89010
2670	Chuvashia	2013.12.06	18:05–18:53	3.020	2.887	19.0	1.37	KOOLS	HD1368
		2013.12.08	19:12–20:40	3.021	2.860	19.0	1.26–1.38	KOOLS	HD1368, SA102-1081
		2014.01.28	17:42–18:01	3.053	2.253	12.6	1.31	KOOLS	SA102-1081
3037	Alku	2013.12.06	18:05–18:53	2.213	1.500	21.5	1.05–1.06	KOOLS	HD28099, HD89010
3104	Durer	2013.04.06	08:18–10:11	3.120	2.236	10.2	1.01–1.09	IRCS	SA102-1081
4896	Tomoegozen	2013.12.08	10:31–11:41	2.655	2.053	19.2	1.03–1.05	KOOLS	HD25680, HD65523, HD70088
4925	Zhoushan	2013.12.08	12:18–15:37	2.454	1.481	4.5	1.04–1.14	KOOLS	HD25680, HD65523, HD70088

\*The heliocentric distance ( $R_h$ ), geocentric distance ( $\Delta$ ), and phase angle ( $\alpha$ ) for asteroid observations were obtained from the NASA/Jet Propulsion Laboratory (JPL) HORIZONS ephemeris generator system.<sup>3</sup>

## 2.1 Near-infrared spectroscopic observations

Spectroscopic data in near-infrared wavelength regions were obtained using the infrared camera and spectrograph (IRCS; Tokunaga et al. 1998; Kobayashi et al. 2000) attached to the f/12 Cassegrain focus of the 8.2 m Subaru Telescope. The instrument detector has a  $1024 \times 1024$  Aladdin-III InSb array, which provides a  $54'' \times 54''$  field-of-view, with a pixel scale of  $0''.052$ . The IRCS system is composed of a number of grisms. Spectroscopic data are obtained by dividing the spectral range into two wavelength regions: *JH* and *HK*. The two wavelength ranges determined using the *JH* grism with the order-sorting filter for *JH* mode and the *HK* grism with the order-sorting filter for *HK* mode were  $1.0\text{--}1.6 \mu\text{m}$  and  $1.45\text{--}2.5 \mu\text{m}$  respectively. There is an overlap wavelength of the two grism modes in  $1.45\text{--}1.60 \mu\text{m}$ . The IRCS in low resolution has a dispersion of approximately  $13 \text{ \AA}$  per pixel in the *JH* grism, and approximately  $12 \text{ \AA}$  per pixel in the *HK* band grism, in the wavelength direction. The orientation of the slit of most observations was along the parallactic angle to prevent the flux loss caused by atmospheric dispersion. To increase the signal-to-noise ratio and avoid the flux loss due to the slit, a 188-element curvature sensor adaptive optics (AO188) system (Minowa et al. 2010) was used with IRCS observations. Since the target asteroids were too faint, the nearby bright stars were used as the natural guide star to operate the AO188 system. Typical seeing size with the AO188 system was improved to  $\sim 0''.2\text{--}0''.6$  in *K* band through the observations.  $0''.3$ ,  $0''.6$ , and  $0''.9$ -wide slits were used according to the changes in the seeing size. The length of each width component of the long slit for IRCS was  $\sim 15''$  in the cross-wavelength direction. The spectral resolution in low dispersion in *JH* and *HK* grisms was  $\sim 100 \text{ \AA}$  in case of using the  $0''.9$  slit.

## 2.2 Visible spectroscopic observations

Optical spectroscopic data were recorded using the Kyoto Okayama Optical Low-dispersion Spectrograph (KOOLS; Ohtani et al. 1998; Ishigaki et al. 2004) installed at the f/18 Cassegrain focus of the 1.88 m telescope at the Okayama Astrophysical Observatory. The  $2048 \times 4096$  SiTe ST-002A CCD installed on KOOLS with  $15 \mu\text{m}$  square pixels, produces a  $5' \times 4.4'$  field-of-view with a pixel scale of  $0''.3$ . A grism with the  $6563 \text{ \AA mm}^{-1}$  blaze and a Y49 order-sorting filter were used, and the covered spectral range is  $0.47\text{--}0.88 \mu\text{m}$ . The KOOLS has a dispersion of approximately  $3.8 \text{ \AA}$  per pixel in the wavelength direction. The length of the long slit for KOOLS was  $4.4'$  in the cross-wavelength direction. Since the 1.88 m telescope did not have an atmospheric dispersion corrector that can prevent flux loss errors, it was necessary to select a wide slit for KOOLS observations; thus, a large width of  $6''$ , which

yields a spectral resolution of  $32 \text{ \AA}$  was utilized.

## 2.3 Methods of data acquisition for asteroids

To acquire an asteroid image as a point source, non-sidereal trackings were employed for the Subaru and 1.88 m telescopes. As a typical method to obtain the reflectance spectrum of the asteroid, the asteroid flux spectrum is divided by the solar flux spectrum. Therefore, solar analogue stars classified as G or F8 stars in the SIMBAD Astronomica database<sup>2</sup> or Drilling & Landolt (1979) were used as standard stars. Observations of the solar analogue stars were coordinated so that the airmass difference between the asteroid and the solar analogue star was less than 0.1 in each case. Spectroscopic observations were performed with an airmass lower than 1.4 to prevent the airmass mismatch between the asteroid and solar analogue star. The asteroids and solar analogue stars were situated in the center of the slit during spectroscopic observations to avoid flux envelope loss due to slits. To reduce noise in signals due to atmospheric emission lines and thermal emissions, spectroscopic data were alternated between two different slit positions, “A” and “B” positions, on the detector. An observation set for the asteroids was composed of four positions, “A–B–B–A”. The “A–B–B–A” sequence for IRCS and KOOLS observations was conducted using the two-position nodding patterns with an interval of  $7''$  and  $20''$  along the cross-wavelength direction of the slit, respectively. The spectrum on the obtained image was recurrently located on the same column to ensure the reproducibility signal. For IRCS and KOOLS observations, flat-fielding images were obtained with a halogen lamp. Wavelength calibration frames for IRCS and KOOLS were acquired regularly at night with light from argon and iron–neon–argon hollow cathode lamps, respectively.

## 2.4 Data reduction procedures

Reduction procedures for all spectroscopic data were conducted using the image reduction and analysis facilities (IRAF) software. For sensitivity correction of each pixel, each object frame for asteroids and solar analogue stars was divided by the flat-fielding frame. The spectra were reduced by subtracting “A” and following “B” images to eliminate the sky background including the emission lines and thermal emissions. The two-dimensional spectrum on the image was collapsed to one-dimensional spectrum using the *apall* task with the IRAF software. Next, wavelength reference positions were determined by adapting the wavelength calibration frame to the object frame. The reflectance of the asteroid was calculated by dividing the spectrum of the asteroid into that of the solar analogue star. Individual visible and near-infrared spectra were smoothed by

<sup>3</sup> (<http://ssd.jpl.nasa.gov/horizons.cgi#top>).

<sup>2</sup> (<http://simbad.u-strasbg.fr/simbad/>).

taking the median of the final reflectance spectrum of each frame, which was normalized to 0.55 and 1.60  $\mu\text{m}$  respectively.

### 3 Obtained spectra and taxonomic classification of asteroids

The spectra of the asteroids taken in this study are shown in figure 1–3. The figures also show the spectra obtained in Kasuga et al. (2013, 2015). Spectroscopic and spectrophotometric data in visible and near-infrared wavelength regions reported in past studies (Zellner, Tholen, & Tedesco 1985; Sykes et al. 2000<sup>4</sup>; Baudrand et al. 2001; Bus & Binzel 2002a; Baudrand, Bec-Borsenberger, & Borsenberger 2004; Lazzaro et al. 2004; Carvano et al. 2010; Clark et al. 2010; Fornasier et al. 2014; Popescu et al. 2016) are also displayed in figure 1–3. Spectral data with wavelength gaps were interpolated to match both levels. The dotted line in the figure is the line used for interpolation between the individual wavelength gap data.

The validity of the method in acquiring the visible spectrum of asteroids using KOOLS is shown by comparing the results with the data from the other studies (Hasegawa et al. 2014). The consistency between the visible spectrum of 3037 Alku in this study (figure 3) and that in Bus & Binzel (2002a) also supports the validity of the method. However, the legitimacy of obtaining near-infrared spectral data of asteroids using IRCS with the AO188 system was not disclosed. To validate the observational methods using IRCS with the AO system, observations for 419 Aurelia, which has a continuous spectrum from 0.3–3.5  $\mu\text{m}$  (Clark et al. 2010; Usui et al. 2019), were taken, although it was not in a photometric condition. The spectra of 419 Aurelia in this study (figure 3) are consistent with those in Clark et al. (2010), which indicates that obtaining the spectra using IRCS with the AO188 system is the proper method.

The observed asteroids were classified to determine the nature of the bright C-complex asteroids. To classify the asteroids with only visible data and both visible and near-infrared data, the Bus taxonomy (Bus & Binzel 2002b) and Bus–DeMeo taxonomy (DeMeo et al. 2009; Binzel et al. 2019) were employed, respectively. Based on the Bus taxonomy, nine asteroids were classified by best fitting the mean visible spectra, which are listed on table III in Bus & Binzel (2002b), to those data. The Bus–DeMeo taxonomy for eighteen asteroids were carried out adapting those data into a taxonomic tool available on the web<sup>5</sup>. When classifying, obvious false data in the spectra due to strong atmospheric absorption between the *Y* and *J* bands, between the *J* and *H* bands, and between the *H* and *K* bands, were corrected by linear interpolation using the appropriate spectra around them. The Bus–DeMeo classification for five asteroids

with visible spectra and near-infrared photometric data in *J*, *H*, and *K<sub>S</sub>* bands were conducted extrapolating the value in the *K<sub>S</sub>* band to the value at 2.45  $\mu\text{m}$ . Note that both taxonomies are based on the spectral shape only, and geometric albedo is not taken into account for the classification.

The classification results for bright C-complex, T-type, and unknown spectral type asteroids and for dark (albedo values less than 0.1) asteroids in the Bus and Bus–DeMeo taxonomy are shown in table 2. The results of the Bus classifications for 2250 Stalingrad, 2310 Olshaniya, 2670 Chuvashia, and 4925 Zhoushan could not be narrowed down to one spectral type due to poor quality of the observed data. By the Bus–DeMeo classification, Asteroid 555 Norma was classified as “indeterminate” using both visible and near-infrared spectra, but was also done as C-type using only near-infrared spectrum.

<sup>4</sup> The latest version is available from Sykes, M. V., Cutri, R., M., Skrutskie, M. F., Fowler, J. W., Tholen, D. J., Painter, P. E., Nelson, B., & Kirkpatrick, D. J. 2010, NASA Planetary Data System, EAR-A-10054/10055-5-2MASS-V2.0.

<sup>5</sup> (<http://smass.mit.edu/busdemeoclass.html>).

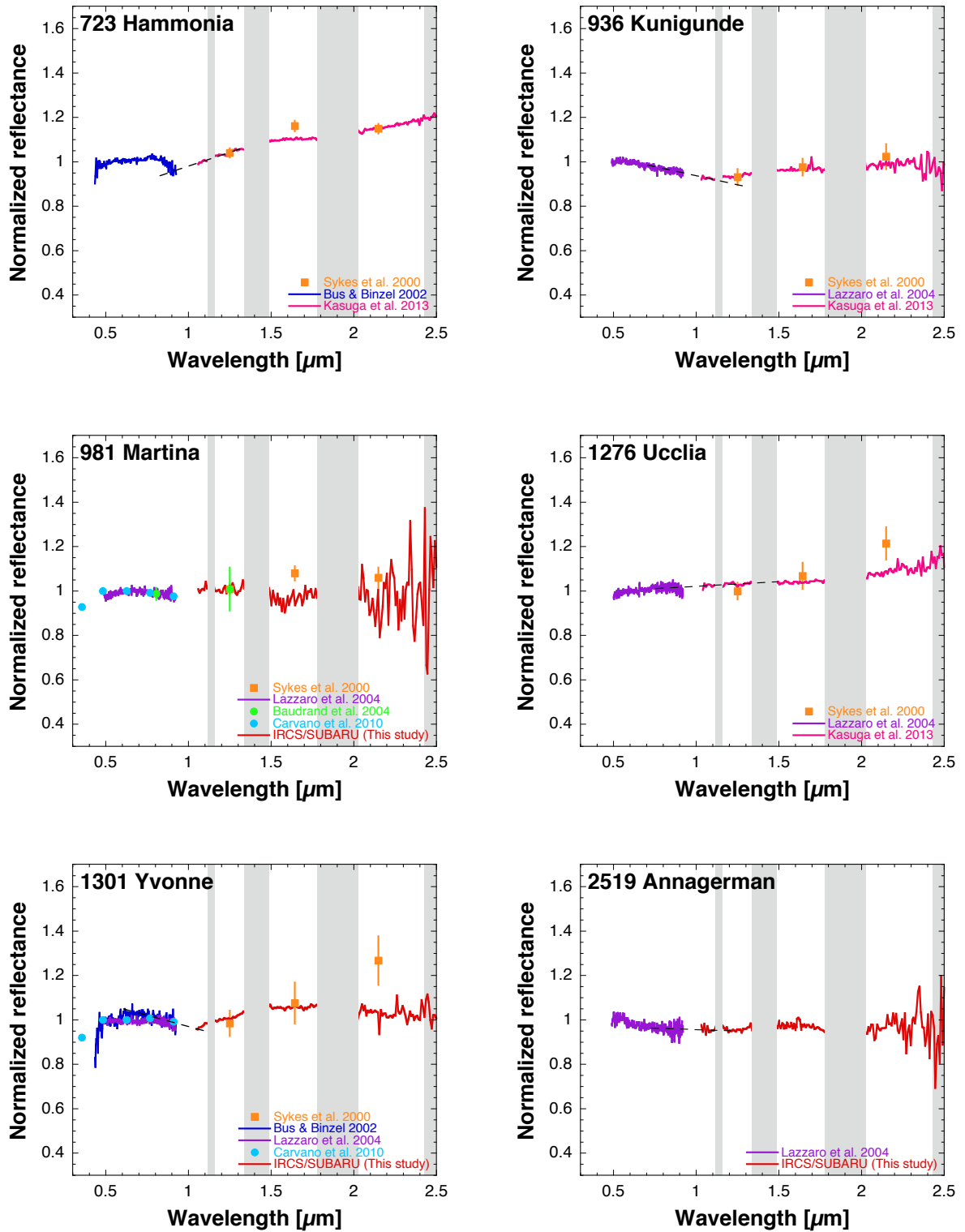


Fig. 1. Reflectance spectra of Bright C-complex and T-type asteroids in the Bus taxonomy. The gray regions around 1.15, 1.40, 1.90, and 2.50  $\mu\text{m}$  indicate the wavelengths affected by the strong absorption due to the terrestrial atmosphere.



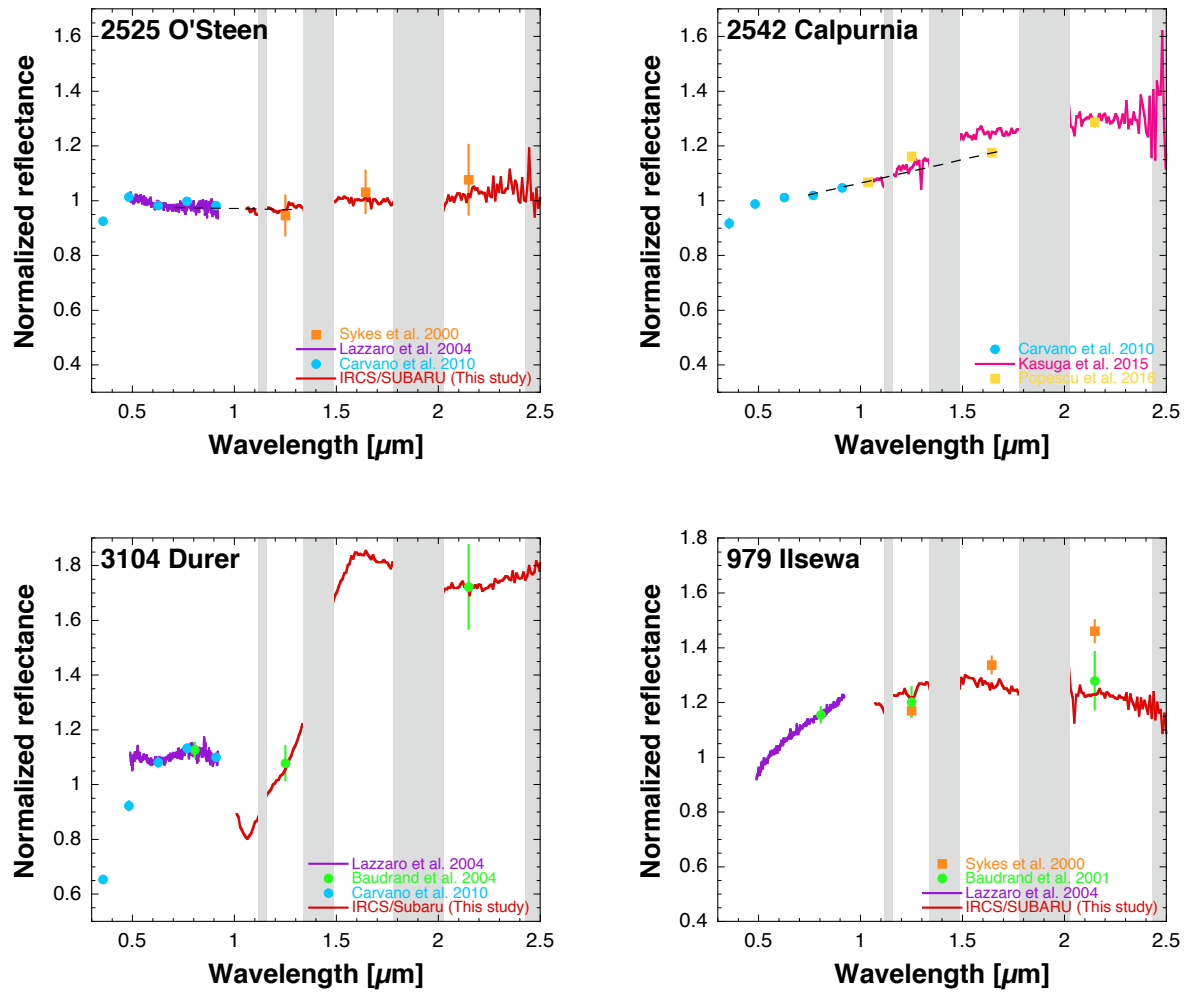
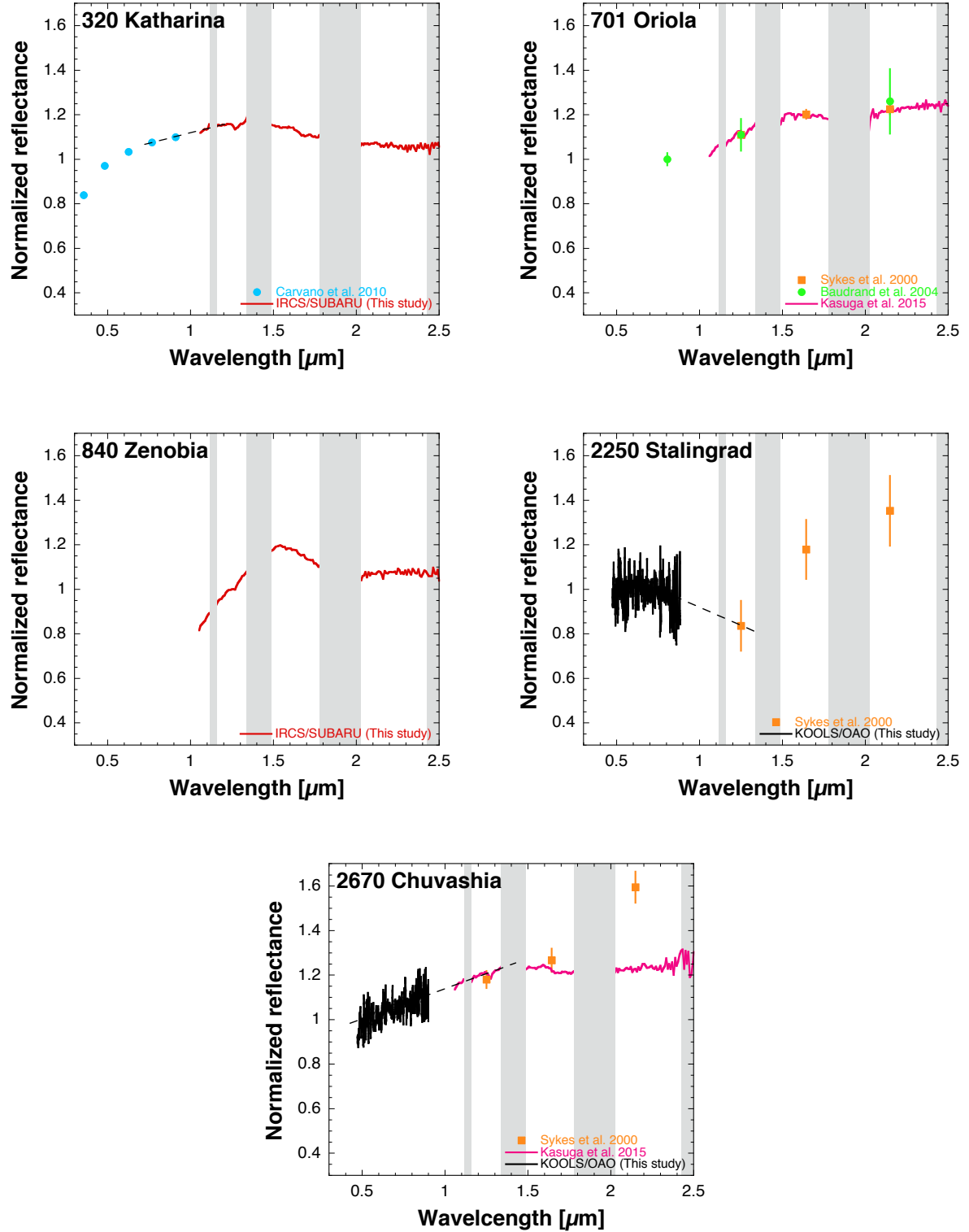


Fig. 1. Continued



**Fig. 2.** Same as figure 1 but for unknown spectral type asteroids with high albedo in the Bus taxonomy. The reflectance is normalized at  $0.55 \mu\text{m}$  except in the case of asteroid 701 Oriola and 840 Zenobia. The reflectance of asteroid 701 Oriola and 840 Zenobia are normalized at  $0.8$  and  $1.25 \mu\text{m}$  respectively.



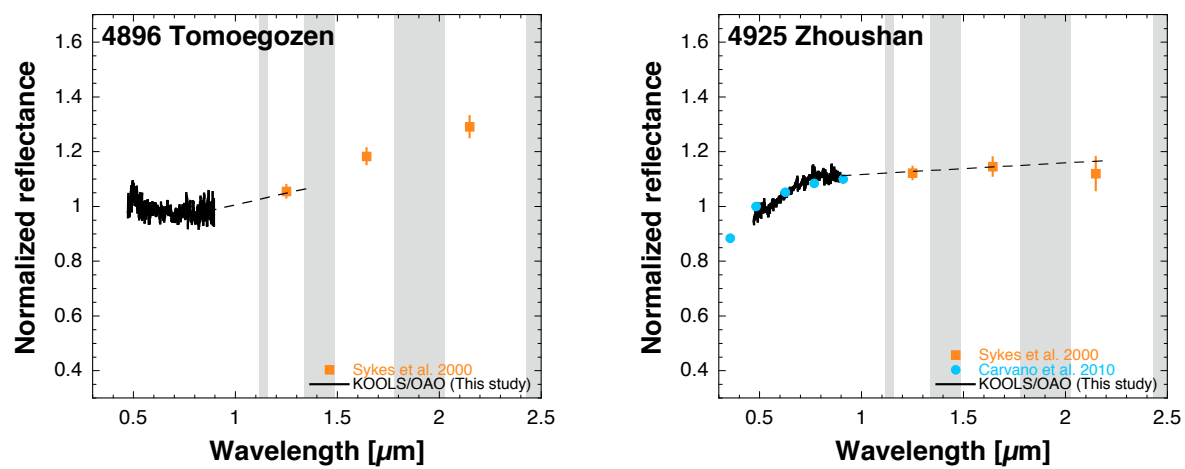


Fig. 2. Continued

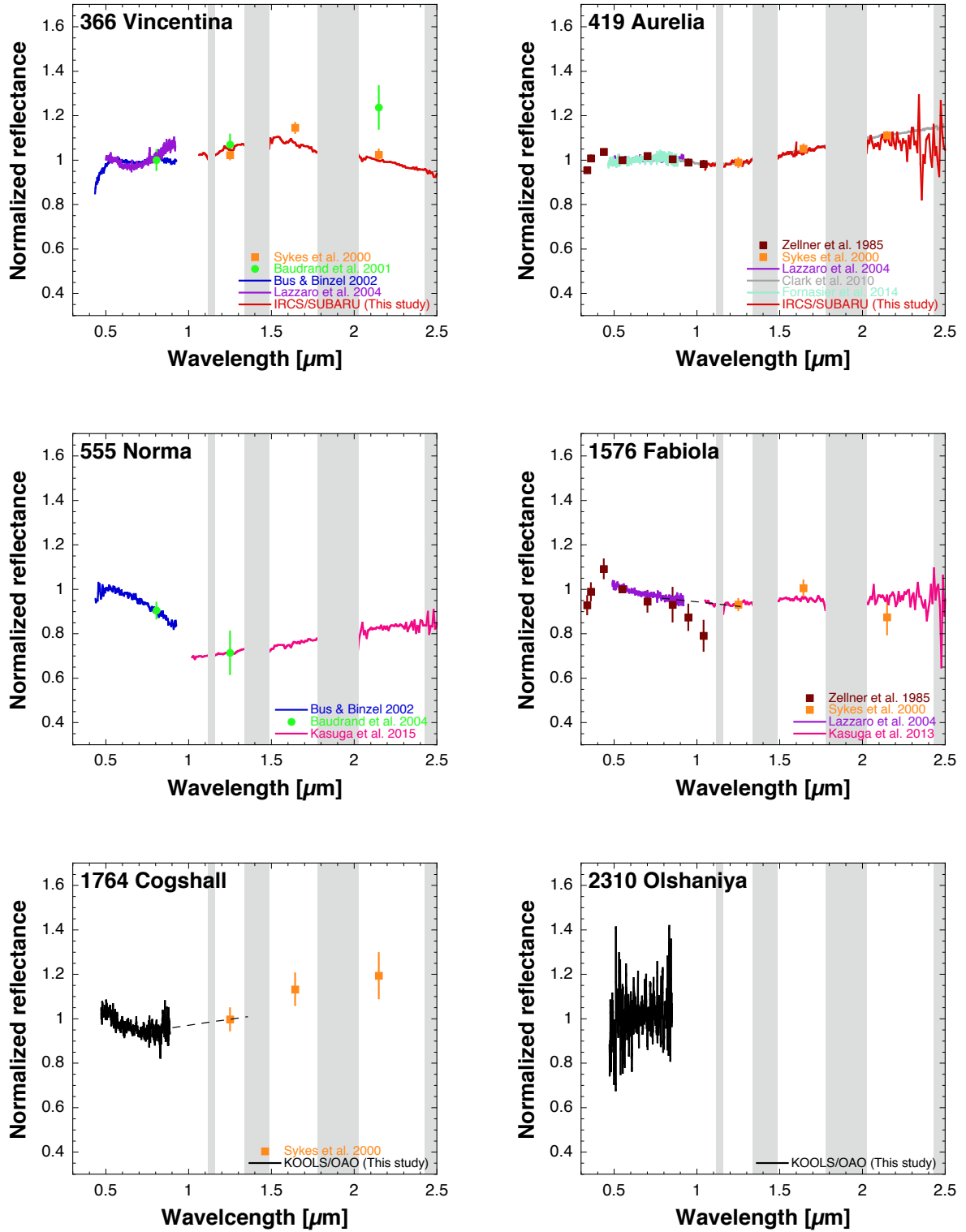


Fig. 3. Same as figure 1 but for asteroids with low albedo.

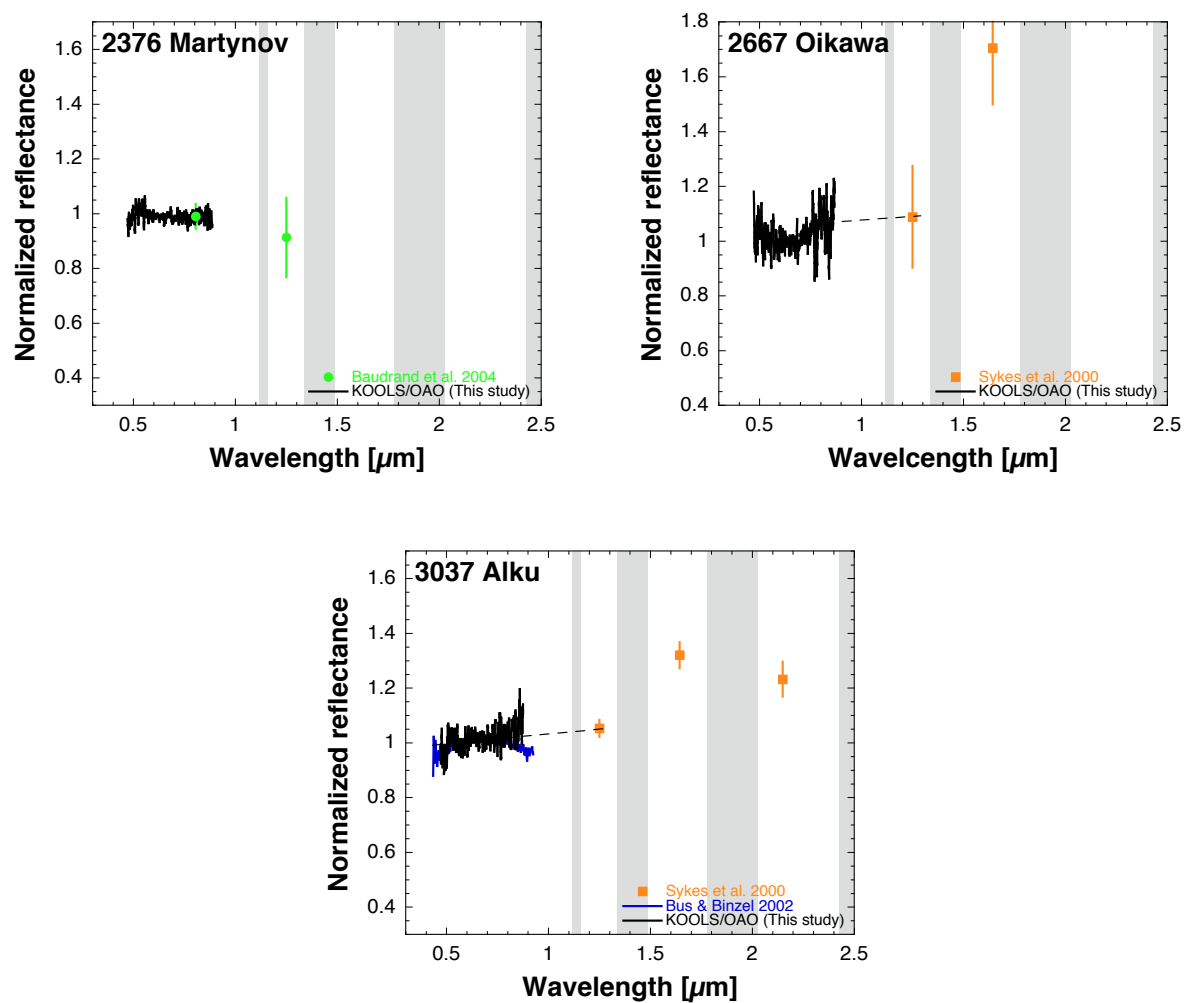


Fig. 3. Continued

**Table 2.** The Bus and Bus–DeMeo taxonomy of the asteroids in this study.

No.	Name	Geometric albedo*			Previous tax <sup>†</sup>	Bus tax	DeMeo tax	<i>a</i> [au]	<i>e</i>	<i>i</i> [°]	Family <sup>‡</sup>
		AKARI	IRAS	WISE							
723	Hammonia	<b>0.294</b>	<b>0.183</b>	<b>0.352</b>	C(B02)	—	<b>Xn</b>	2.9935	0.0596	4.982	
936	Kunigunde	<b>0.124</b>	<b>0.113</b>	0.065	B(L04)	—	<b>C</b>	3.1302	0.1786	2.371	Themis
981	Martina	<b>0.108</b>	<b>0.125</b>	0.084	B(L04)	—	<b>B</b>	3.0950	0.2038	2.067	Themis
1276	Ucclia	<b>0.141</b>	<b>0.130</b>	0.053	C(L04)	—	<b>C</b>	3.1726	0.1021	23.345	Alauda
1301	Yvonne	<b>0.201</b>	<b>0.163</b>	<b>0.181</b>	C(B02), Cb(L04), <i>C<sub>p</sub></i> (C10) <sup>1</sup>	—	<b>K</b>	2.7623	0.2734	34.066	
2519	Annagerman	<b>0.105</b>	—	<b>0.115</b>	Ch(L04)	—	<b>B</b>	3.1390	0.1739	2.423	Themis
2525	O'Steen	<b>0.124</b>	—	0.098	B(L04), <i>C<sub>p</sub></i> (C10) <sup>1</sup>	—	<b>Cb</b>	3.1378	0.1906	2.774	Themis
2542	Calpurnia	<b>0.146</b>	0.064	<b>0.102</b>	<i>C<sub>p</sub></i> (C10) <sup>1</sup>	—	<b>Xk</b>	3.1296	0.0738	4.621	
3104	Durer	<b>0.237</b>	—	<b>0.357</b>	Ch(L04), <i>A<sub>p</sub></i> (C10) <sup>1</sup>	—	<b>Sa</b>	2.9616	0.0914	24.187	
979	Ilsewa	<b>0.142</b>	<b>0.157</b>	<b>0.139</b>	T(L04)	—	<b>L</b>	3.1655	0.1339	10.058	
320	Katharina	<b>0.165</b>	—	<b>0.152</b>	<i>DL<sub>p</sub></i> (C10) <sup>1</sup>	—	<b>Xe</b>	3.0096	0.1172	9.379	Eos
701	Oriola	<b>0.239</b>	<b>0.218</b>	<b>0.124</b>	—	—	<b>K</b>	3.0142	0.0336	7.143	
840	Zenobia	<b>0.610</b>	—	<b>0.313</b>	—	—	<b>Sq</b>	3.1298	0.1007	9.989	
2250	Stalingrad	<b>0.121</b>	—	<b>0.120</b>	—	<b>B, Cb</b>	(C) <sup>§</sup>	3.1908	0.1801	1.524	Themis
2670	Chuvashia	<b>0.302</b>	—	<b>0.246</b>	—	X, Xe	<b>Xe</b>	3.1688	0.0733	9.857	
4896	Tomoegezen	<b>0.135</b>	—	<b>0.136</b>	—	<b>B</b>	(C) <sup>§</sup>	3.1070	0.1701	16.565	
4925	Zhoushan	<b>0.181</b>	—	<b>0.195</b>	<i>XL<sub>p</sub></i> (C10) <sup>1</sup>	<b>Xe, Xk</b>	(Xe) <sup>§</sup>	3.0459	0.2491	8.344	
366	Vincentina	0.097	0.080	0.079	Ch(B02, L04)	—	<b>K</b>	3.1492	0.0554	10.562	
419	Aurelia	0.051	0.046	—	F(T84), Cb(L04), C(D09)	—	<b>C</b>	2.5958	0.2522	3.924	
555	Norma	<b>0.101</b>	0.063	0.096	B(B02)	—	Indet., <b>C</b>	3.1844	0.1572	2.637	
1576	Fabiola	<b>0.100</b>	0.091	0.075	BU(T84), B(L04)	—	<b>B</b>	3.1390	0.1752	0.944	Themis
1764	Cogshall	0.094	0.085	0.061	—	<b>B</b>	(C) <sup>§</sup>	3.0945	0.1205	2.235	Themis
2310	Olshaniya	0.083	0.050	0.064	—	<b>C, Xc</b>	—	3.1432	0.1613	2.650	Themis
2376	Martynov	0.042	0.054	0.034	—	<b>Ch</b>	—	3.2032	0.1178	3.838	
2667	Oikawa	0.041	0.043	—	—	<b>B</b>	—	3.2252	0.1884	2.238	Themis
3037	Alku	0.061	0.113	0.034	C(B02)	<b>C</b>	(C) <sup>§</sup>	2.6754	0.1872	18.980	

Top panel: bright C-complex asteroids; second panel: a bright T-type asteroid; third panel: unknown spectral type asteroids; bottom panel: dark asteroids.

\*References for geometric albedos: AKARI, Usui et al. (2011); IRAS, Tedesco et al. (2002); WISE, Masiero et al. (2011, 2012).

<sup>†</sup>References for taxonomy: T84, Tholen (1984); B02, Bus & Binzel (2002b); L04, Lazzaro et al. (2004); C10, Carvano et al. (2010).

<sup>‡</sup>Data for asteroid family are quoted from D. Nesvorný, (2015)<sup>5</sup>.

<sup>§</sup>The Bus–DeMeo taxonomic result for the asteroid was acquired by extrapolating the value in  $K_S$  band to the value at 2.45  $\mu\text{m}$ .

The DeMeo C-type asteroids include asteroids classified in Bus B-type (see table 3 in this study; DeMeo et al. 2009; de León et al. 2012). In this work, these objects are called C-type asteroids with concave curvature. About one third of the known C-types (DeMeo) asteroids (DeMeo et al. 2009; Clark et al. 2010; Ostrowski et al. 2011; de León et al. 2012; Hasegawa et al. 2017, 2018; Binzel et al. 2019) are C-types with concave curvature. It is possible that these data are subject to selection bias, nevertheless, it is worth noting that Bus B-type asteroids are not always classified as DeMeo B-type asteroids. This is because the Bus B-type asteroids do not necessarily have concave curvature over the range from the visible to near-infrared. The Bus B-type asteroids with a flat or convex curvature in the near-infrared are typically classified as DeMeo C-type.

The Bus–DeMeo taxonomic results from both visible and near-infrared spectra for bright C-complex asteroids show that the existence of DeMeo X-complex and C-type with concave curvature, B-, Cb-, K-, and Sa-type (see top of table 2). Bright T-type (Bus) asteroids were classified as L-type (DeMeo) in this study (see second panel of table 2). Bright asteroids with unknown spectrum type were identified as DeMeo X-complex, K-, Sq-, and C-type with concave curvature (see third panel of table 2).

#### 4 The boundaries of albedoes for bright C-complex asteroids

In order to find appropriate albedo boundaries between the dark and the bright C-complex asteroids, the distributions of the geometric albedo for B-, Ch-, and C-types (Bus) were derived. The geometric albedo values of asteroids are available in literature (AKARI: Usui et al. 2011; Hasegawa et al. 2013; IRAS: Tedesco et al. 2002; WISE: Grav et al. 2011, 2012; Mainzer et al. 2011a; Masiero et al. 2011, 2012, 2014). The classification results, based on the Bus taxonomy are quoted from Bus & Binzel (2002b); Lazzaro et al. (2004); Binzel et al. 2001, 2004; Rivkin et al. (2003); Yang et al. (2003); Lazzarin et al. (2004a, 2004b, 2005); Marchi et al. (2005); Davies et al. (2007); Moskovitz et al. (2008a, 2008b); Mothé-Diniz & Nesvorný (2008a, 2008b); Roig et al. (2008); Duffard & Roig (2009); Iwai et al. (2017). Most asteroids in this study are main-belt asteroids with diameters larger than 10 km. The albedo distributions are shown in figure 4.

In the beginning, we focus on the B-type asteroids. Figure 4 (left) indicate the existence of bright B-type asteroids. Alí-Lagoa et al. (2016) reports that the albedo of the members of the Pallas family occupied by B-type asteroids is  $0.141 \pm 0.043$ . The presence of bright B-type asteroids (Bus) in the Pallas family (table 3) supports the result of Alí-Lagoa et al. (2016). As

a result of applying the two-component Gaussian distribution to B-type asteroids, the mean value of the high-albedo part for B-type asteroids is 0.164, which is consistent with the result of Alí-Lagoa et al. (2016). The boundary value of the albedo of between the bright and dark B-type asteroids is derived as 0.098. All B-type asteroids in the Bus taxonomy with albedo values larger than 0.1 are listed in table 3.

Next, the albedo distribution for Bus Ch- and C-type asteroids was statistically evaluated. In order not to underestimate values of the standard deviation for Ch and C-type (Bus) asteroids, they were obtained without using Gaussian distribution fitting. The mean and standard deviation of  $\log(\text{albedo})$  for Ch-type asteroids are  $-1.261 = \log(0.065)$  and 0.160, respectively. The mean and standard deviation of  $\log(\text{albedo})$  for C-type asteroids are  $-1.225 = \log(0.060)$  and 0.207, respectively. Even if the asteroid has an albedo value exceeding 0.1 into the  $2\sigma$  range (Ch-type: less than 0.115, C-type: less than 0.154), it is considered to be a normal Ch- or C-type asteroid. Figure 4 (middle and right) shows the results of the albedo distribution for Ch- and C-type (Bus) asteroids. Almost no Ch- and C-type (Bus) asteroids with an albedo value below  $-2\sigma$  exist, but there are several Ch- and C-type (Bus) asteroids with albedo values larger than  $+2\sigma$ . Since Bus Ch- and C-type asteroids with an albedo value within  $+2\sigma$  can be considered normal Ch- and C-type (Bus) asteroids, we next consider the nature of bright Ch- and C-type (Bus) asteroids with an albedo value exceeding  $+2\sigma$ . The boundary values of the albedos of between the bright and dark Ch-type asteroids and between the bright and dark C-type asteroids are derived as 0.115 and 0.154. All Ch- and C-type asteroids in the Bus taxonomy with albedo values larger than 0.115 and 0.154 are listed in table 4 and 5, respectively.

## 5 Discussion

### 5.1 Analogue material and meteorites

On the basis of visible and near-infrared spectroscopic results in the literature as well as this study, bright C-complex asteroids are classified as B, C with concave curvature, Xn, and Sq (Bus B-type), Sa (Bus Ch-type), and Xn, K and B (Bus C-type) (table 3, 4, and 5). There are some outliers in these results. For example, Ch-type (Bus) asteroid 3104 Durer is classified into Sa-type in this study, which is consistent with  $A_p$ -type in Carvano et al. (2010). Meanwhile, the spectrum of 3104 Durer in Lazzaro et al. (2004) showed Ch-type (Bus) characteristics. This spectral mismatch may be explained by a misidentification of the target in one of their surveys. For another example, B-type (Bus) asteroid 8567 1996 HW<sub>1</sub> is classified into Sq-type in DeMeo, Binzel, & Lockhart (2014), which is inconsistent with B-type in Lazzarin et al. (2004b). This spectral discrepancy may also be due to misidentification of the target. Except for such S-

<sup>6</sup> Nesvorný, D. 2015, NASA Planetary Data System, EAR-A-VARGBDT-5-NESVORNYFAM-V3.0

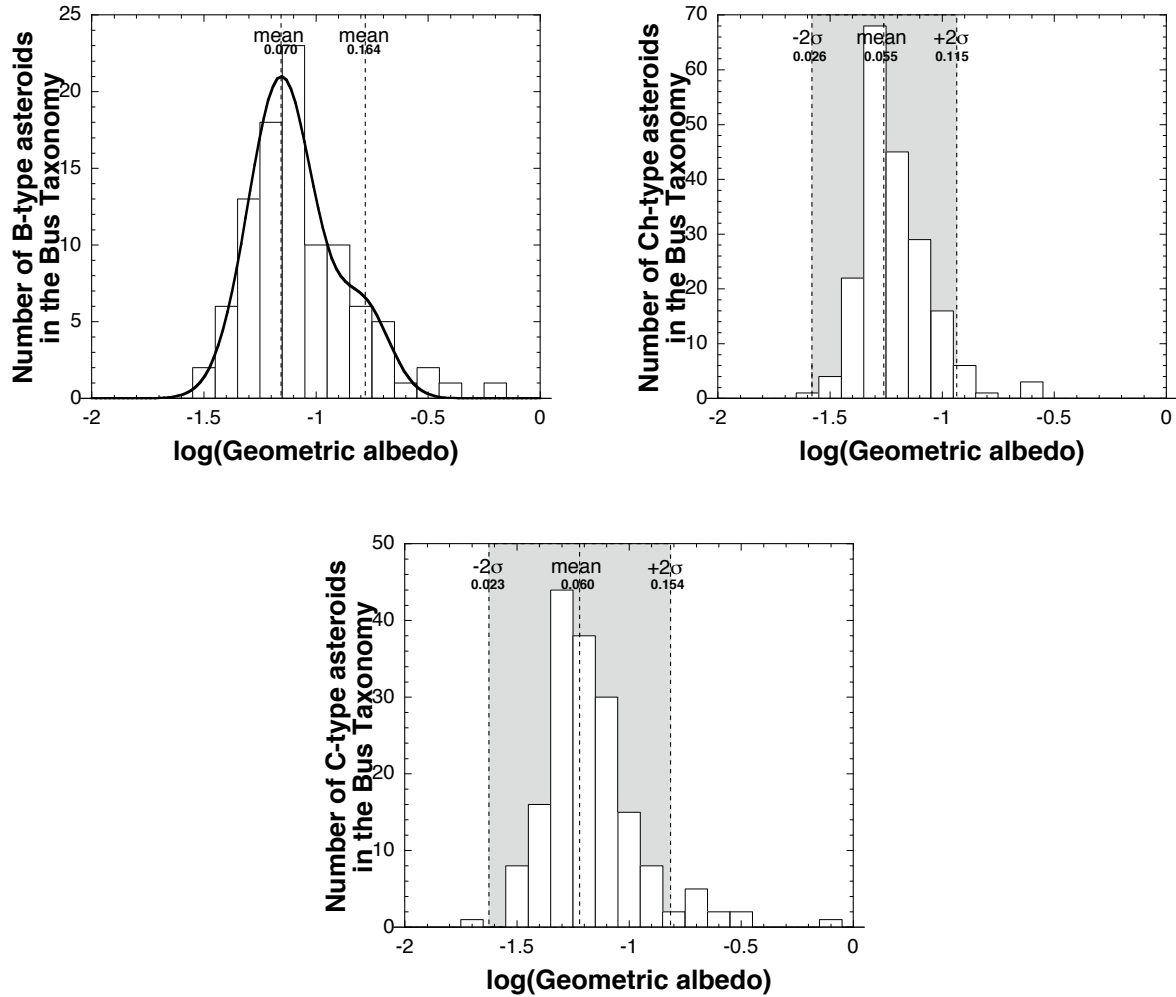


**Fig. 4.** Albedo distribution of B-, Ch-, and C-type asteroids in the Bus taxonomy. The left, middle, and right histograms show the number of B, Ch-, and C-type asteroids in the Bus taxonomy, respectively. The number of samples for B-, Ch-, and C-type are 98, 195, and 172, respectively. The solid line in the figure for B-type asteroids is the best-fitting two-component Gaussian distribution.

complex asteroids, these spectral type asteroids are candidates for the bright C-complex asteroids.

It is known that the spectra of meteorites become bluer with an increase in particle size of regolith layer (e.g., Johnson & Fanale 1973; Vernazza et al. 2016). Hasegawa et al. (2019) argued that the spectra of the Q-type can be explained by lack of fine particles even if space weathering matures their surface. It is expected that originally bright X-complex asteroids with reddish spectra appear to be bright C-complex asteroids due to spectral bluing effect caused by the absence of regolith on their surface. Solar radiation pressure and electrostatic force are known as the effect of removal of fine particles from the asteroid surface layer (Hasegawa et al. 2019). However, these effects can only be worked effectively to near-earth asteroids with less than 0.5 km in diameter. Bright C-complex (Bus) asteroids focused in this study are main-belt asteroids with a diameter of

more than 10 km, so that fine particles on their surface cannot escape since low influence of these forces affects to the particles due to their high gravity and/or few solar flux compared to that around the near-earth space. Therefore, the cause of the existence of bright C-complex (Bus) asteroids cannot be attributed to spectral changes.

Based on meteorite studies (e.g., Hiroi et al. 1993, 1996), bright B-type asteroids are likely to be thermally metamorphosed carbonaceous chondrites. de León et al. (2012) shows that the spectra of B-type asteroids are similar to those of CV3 and CK4 carbonaceous chondrites. Meanwhile, Marsset et al. (2020) shows that the cause of the brighter surface on 2 Pallas may be the distribution of salts in the surface layer. Salts have already been found on 1 Ceres (De Sanctis et al. 2016), and their presence has also been proposed for the Trojan asteroids (Yang, Lucey, & Glotch 2013). Xn-type (DeMeo) asteroids are min-

**Table 3.** Bright B-type asteroids in the Bus taxonomy.

No.	Name	Bus Tax*	DeMeo Tax*	Geometric albedo <sup>†</sup>			Remark
				AKARI	IRAS, etc	WISE	
2	Pallas	B(B02)	B(D09)	<b>0.159</b>	<b>0.143</b>	<b>0.142</b>	Pallas <sup>‡</sup>
214	Aschera	B(L04), Xc(B02)	Xn(H17)	<b>0.419</b>	<b>0.522</b>	<b>0.210</b>	
383	Janina	B(B02)	C(C110)	<b>0.133</b>	0.093	0.096	Themis <sup>‡</sup>
400	Ducrosa	B(L04)	—	<b>0.149</b>	<b>0.142</b>	<b>0.153</b>	
531	Zerlina	B(B02)	B(d12)	<b>0.185</b>	<b>0.146</b>	<b>0.101</b>	Pallas <sup>‡</sup>
621	Werdandi	B(L04)	—	<b>0.124</b>	<b>0.153</b>	<b>0.127</b>	Themis <sup>‡</sup>
936	Kunigunde	B(L04)	C(This study)	<b>0.124</b>	<b>0.113</b>	0.065	Themis <sup>‡</sup>
981	Martina	B(L04)	B(This study)	<b>0.108</b>	<b>0.125</b>	0.084	Themis <sup>‡</sup>
1003	Lilofee	B(L04)	C(d12)	<b>0.198</b>	( <b>0.212</b> ) <sup>§</sup>	<b>0.151</b>	Themis <sup>‡</sup>
1101	Clematis	B(L04)	—	<b>0.190</b>	<b>0.112</b>	<b>0.127</b>	Alauda <sup>‡</sup>
1331	Solvejg	B(B02)	—	<b>0.159</b>	<b>0.151</b>	0.099	
1487	Boda	B(L04)	—	<b>0.133</b>	<b>0.120</b>	0.097	Themis <sup>‡</sup>
1539	Borrelly	B(B02)	C(d12)	<b>0.166</b>	(0.074) <sup>§</sup>	<b>0.142</b>	Themis
1705	Tapio	B(B02)	C(d12)	<b>0.100</b>	<b>0.118</b>	0.089	
2382	Nonie	B(B02)	—	<b>0.120</b>	—	<b>0.113</b>	Pallas <sup>‡</sup>
2464	Nordenskiöld	B(L04)	—	0.098	<b>0.150</b>	0.083	
2525	O’Steen	B(L04)	Cb(This study)	<b>0.124</b>	—	0.098	Themis <sup>‡</sup>
3000	Leonardo	B(B02)	—	—	—	<b>0.148</b>	
3036	Krat	B(L04)	C(d12)	<b>0.116</b>	<b>0.118</b>	0.091	Alauda <sup>‡</sup>
3348	Pokryshkin	B(I17) <sup>  </sup>	—	<b>0.126</b>	—	<b>0.126</b>	
3200	Phaethon	B(B02)	B(d12)	<b>0.160</b>	<b>0.107</b>	<b>0.16</b>	Apollo <sup>‡</sup>
3579	Rockholt	B(B02)	—	—	—	<b>0.120</b>	$i = 31.1^\circ$
4100	Sumiko	B(L04)	—	<b>0.156</b>	—	<b>0.201</b>	Eos <sup>‡</sup>
4396	Gressmann	B(B02)	—	—	—	<b>0.288</b>	
4896	Tomoegozen	B(This study)	—	<b>0.135</b>	<b>0.102</b>	<b>0.136</b>	
4997	Ksana	B(B02)	—	<b>0.312</b>	—	<b>0.316</b>	Pallas <sup>‡</sup>
5222	Ioffe	B(B02)	—	<b>0.139</b>	<b>0.146</b>	<b>0.144</b>	Pallas <sup>‡</sup>
5234	Sechenov	B(B02)	—	<b>0.213</b>	—	<b>0.157</b>	Pallas <sup>‡</sup>
5330	Senrikyu	B(B02)	—	<b>0.201</b>	<b>0.223</b>	<b>0.123</b>	Pallas <sup>‡</sup>
5639	1989 PE	B(L04)	—	<b>0.117</b>	—	<b>0.198</b>	$i = 26.6^\circ$
5870	Baltimore	B(L04)	—	<b>0.249</b>	<b>0.215</b>	—	Mars-crosser <sup>‡</sup>
6500	Kodaira	B(B02)	—	—	—	<b>0.150</b>	Mars-crosser <sup>‡</sup>
8567	1996 HW <sub>1</sub>	B(Ln04b)	Sq(D14)	—	—	<b>0.160</b>	Amor <sup>‡</sup>
9222	Chubey	B(M08)	—	—	—	<b>0.408</b>	Tirela <sup>‡</sup>
49591	1999 DO <sub>2</sub>	B(I17) <sup>  </sup>	—	—	—	<b>0.119</b>	
94030	2000 XC <sub>40</sub>	B(I17) <sup>  </sup>	—	—	—	<b>0.109</b>	$i = 28.0^\circ$

\*References for taxonomy: B02, Bus & Binzel (2002b); L04, Lazzaro et al. (2004); Ln04b, Lazzarin et al. (2004b); M08, Mothé-Diniz & Nesvorný (2008a); D09, DeMeo et al. (2009); C110, Clark et al. (2010); D12, de León et al. (2012); D14, DeMeo, Binzel, & Lockhart (2014); H17, Hasegawa et al. (2017); I17, Iwai et al. (2017).

<sup>†</sup>References for geometric albedos: AKARI, Usui et al. (2011); IRAS, Tedesco et al. (2002); WISE, Masiero et al. (2011, 2012, 2019).

<sup>‡</sup>Data for asteroid family are quoted from D. Nesvorný, (2015)<sup>6</sup> and data except families were obtained from the NASA JPL HORIZON ephemeris generator system<sup>3</sup>.

<sup>§</sup>The values are obtained by not IRAS but the NASA Infrared Telescope Facility (Tedesco, Cellino, & Zappalà 2005).

<sup>||</sup>Based on the Bus taxonomy, the classifications are re-performed in this study.

erologically associated with enstatite chondrites and/or achondrites (e.g., Lucas et al. 2019), as also reported in Kasuga et al. (2013, 2015). Enstatite chondrite and/or achondrites are formed in a high-degree reductive environment and a high temperature

environment such as in internal igneous or external large-scale impact melting processes (e.g., Keil 1989, 2010). Neeley et al. (2014) suggested that DeMeo Xk-type asteroids are related to iron meteorites, enstatite chondrites, and stony-iron meteorites,



**Table 4.** Bright Ch-type asteroids in the Bus taxonomy.

No.	Name	Bus	DeMeo	Geometric albedo <sup>†</sup>			Remark <sup>*</sup>
		Tax <sup>*</sup>	Tax <sup>*</sup>	AKARI	IRAS	WISE	
1694	Kaiser	Ch(L04)	—	<b>0.241</b>	—	<b>0.166</b>	
2428	Kamenyar	Ch(B02)	—	<b>0.139</b>	0.086	<b>0.116</b>	$C_p(C10)$ , Veritas <sup>‡</sup>
3104	Durer	Ch(L04)	Sa(This study)	<b>0.237</b>	—	<b>0.357</b>	$A_p(C10)$ , $i = 24.2^\circ$
4284	Kaho	Ch(B02)	—	<b>0.125</b>	—	<b>0.128</b>	$C_p(C10)$
4621	Tambov	Ch(L04)	—	—	—	<b>0.234</b>	

<sup>\*</sup>References for taxonomy: B02, Bus & Binzel (2002b); L04, Lazzaro et al. (2004); C10, Carvano et al. (2010).

<sup>†</sup>References for geometric albedos: AKARI, Usui et al. (2011); IRAS, Tedesco et al. (2002); WISE, Masiero et al. (2011, 2012).

<sup>‡</sup>Data for asteroid family are quoted from D. Nesvorný, (2015)<sup>6</sup>.

**Table 5.** Bright C-type asteroids in the Bus taxonomy.

No.	Name	Bus	DeMeo	Geometric albedo <sup>†</sup>			Remark <sup>*</sup>
		Tax <sup>*</sup>	Tax <sup>*</sup>	AKARI	IRAS, etc	WISE	
723	Hammonia	C(B02)	Xn(This study)	<b>0.294</b>	<b>0.183</b>	<b>0.352</b>	
1301	Yvonne	C(B02)	K(This study)	<b>0.201</b>	<b>0.163</b>	<b>0.181</b>	$i = 34.1^\circ$
1989	Tatry	C(B02)	—	<b>0.262</b>	—	<b>0.193</b>	
2100	Ra-Shalom	C(B04)	B(B19)	<b>0.177</b>	—	—	Aten <sup>‡</sup>
2331	Parvulesco	C(B02)	—	—	—	<b>0.713</b>	$CX_p(C10)$
2346	Lilio	C(B02)	—	—	—	<b>0.277</b>	
2730	Barks	C(B02)	—	<b>0.196</b>	( <b>0.354</b> ) <sup>§</sup>	<b>0.162</b>	
3137	Horky	C(B02)	—	—	—	<b>0.207</b>	$CX_p(C10)$
3435	Boury	C(B02)	—	<b>0.163</b>	—	<b>0.212</b>	
4107	Rufino	C(B02)	—	<b>0.199</b>	<b>0.318</b>	<b>0.169</b>	
5678	DuBridge	C(B02)	—	—	—	<b>0.332</b>	Pallas <sup>‡</sup>

<sup>\*</sup>References for taxonomy: B02, Bus & Binzel (2002b); C10, Carvano et al. (2010); B19, Binzel et al. (2019).

<sup>†</sup>References for geometric albedos: AKARI, Usui et al. (2011); IRAS, Tedesco et al. (2002); WISE, Masiero et al. (2011, 2012).

<sup>‡</sup>Data for asteroid family are quoted from D. Nesvorný, (2015)<sup>6</sup> and data except families were obtained from the NASA JPL HORIZON ephemeris generator system<sup>3</sup>.

<sup>§</sup>This value was obtained by not IRAS but the NASA Infrared Telescope Facility (Tedesco, Cellino, & Zappalà 2005).

all of which are originated from high-temperature parent bodies. DeMeo K-type asteroids are linked to CK chondrites (Mothé-Diniz et al. 2008; Clark et al. 2009), which are known to be highly oxidized and thermally metamorphosed meteorites (e.g., Greenwood et al. 2010). As described above, we speculate that the bright C-complex asteroids originated from parent bodies of which the interiors were experienced high temperatures. To confirm this hypothesis, we investigate the correlation by adapting the results in this study to the known spectrophotometric data as follows.

## 5.2 Sources of the bright C-complex asteroids

We examine the spectral distribution of some collisional families including bright C-complex asteroids and correlate them with the spectra of the bright C-complex asteroids in order to understand the origin of these asteroids. Since members of asteroid families are considered as fragments ejected from the par-

ent bodies by catastrophic disruption or cratering, it is possible to estimate the composition of the parent bodies from those spectra. The number of spectroscopic data acquired in both the visible and near-infrared wavelength regions for bright C-complex asteroids is still too small and there are not enough numbers of asteroids, even those with visible spectra, to compare the spectroscopic properties of the family members (table 3, 4, and 5). To examine the spectral properties of family members, we use the classification based on the Sloan Digital Sky Survey (SDSS) multicolor photometric data in Carvano et al. (2010). The C-complex asteroids in Carvano et al. (2010) are classified into one class,  $C_p$ -type (photometric C-type). In this study, we define  $C_p$ -complex asteroids as asteroids of not only  $C_p$ -type, but also  $CD_p$ -,  $CL_p$ -, and  $CX_p$ -types, which are intermediate types between  $C_p$  and other spectral types. Bright  $C_p$ -complex asteroids are defined as those with an albedo of more than 0.115 (see section 4), which is the threshold value for bright Ch-type (Bus) asteroids. We also add the defini-

tion of  $B_p$ -type, as B-type asteroids in Alf-Lagoa et al. (2016) among  $C_p$ -complex asteroids. The mean spectral distribution and abundance of families with bright C-complex asteroids present in their members (table 3, 4, and 5) and families having mean low albedo values are shown in figure 5 and table 6, respectively.

The Eos family is known to be bright, which have a mean albedo of more than 0.1 (Masiero et al. 2011) and a mixture of members with various spectra such as K-, Ld-, Xc-, X-, C-, and B-types (Mothé-Diniz, Roig, & Carvano 2005). Some Eos family members have a flat visible spectrum (e.g., 4455 Ruriko, which is identified as a C-complex asteroid by Doressoundiram et al. 1998), have the albedo values of more than 0.1 (Masiero et al. 2011). In this study, bright  $C_p$ -complex asteroids were found to be abundant in the Eos family (table 6). The mean spectrum of bright  $C_p$ -complex asteroids in the Eos family tend to be slightly redder than the spectra of those in other families and also the bright C-complex asteroids in this study (figure 5). Within the Eos family, 55 percent of bright  $C_p$ -complex asteroids are of the  $C_p$ -type, 28 percent is of the  $CX_p$ -type and 14 percent is of the  $CL_p$ -type. This indicates that the bright  $C_p$ -complex asteroids in the Eos family contains the  $X_p$ -type and the  $L_p$ -type asteroids, and is consistent with the fact that the family members have a diverse spectrum (Mothé-Diniz, Roig, & Carvano 2005). The Eos family asteroids are thought to be related to the R-chondrites and CK chondrites (Mothé-Diniz et al. 2008), and these meteorites are known to have formed at high temperature (Weisberg, McCoy, & Krot 2006). Thus, one of the origins of the bright C-complex asteroids is likely to be from asteroids that were formed at high temperature in the interior of the parent bodies. From the models proposed by Greenwood et al. (2010) for the parent bodies of CV and CK chondrites, it is preferable to adopt one with a single parent object and a single collisional event to explain diverse spectra and the power law of the size distribution of the Eos family members.

Bright  $C_p$ -complex asteroids in the Pallas, Themis, and Hygiea families are found to have concave curvature over 0.5–0.9 microns, similar to the bright B-type asteroids (figure 5). Members of these families also include bright  $B_p$ -type asteroids (table 6). Marsset et al. (2020) indicated the possibility of salt deposits on 2 Pallas and that on the Pallas family members as well. The Themis and Hygiea families are located in the outer main-belt, and most of their members have a low albedo of less than 0.1, unlike the Pallas family members (table 6). The Hygiea family is thought to have been formed by a cratering event based on the size distribution of its members (Carruba 2013), while the Themis family was formed by a catastrophic disruption event (Marzari, Davis, & Vanzani 1995), both of which were originated from the parent bodies of similar size to that of 2 Pallas (Vernazza et al. 2020; Marzari, Davis, & Vanzani 1995). The composition of these parent bodies could be CK

and/or R chondrite analogues, such as the Eos family, or salt deposits, such as the 2 Pallas (Marsset et al. 2020). Besides, (a) salts may be present in asteroids in the outer main-belt (Poch et al. 2020), (b) the theory and observations suggest that salts may be present in the Themis parent body (Castillo-Rogez & Schmidt 2010; Marsset et al. 2016), (c) salt precipitation can be explained by small percentages (Castillo-Rogez et al. 2018), thus it is very likely that the parent bodies of the Themis and Hygiea family were as likely to have precipitated salt as 1 Ceres and 2 Pallas. However, the proportion of salts produced in Themis and Hygiea parent bodies is considered to be lower than that in 2 Pallas, because a fraction of bright C-complex asteroids in members of the Themis and Hygiea family are smaller than those of the Pallas family (table 6).

The spectral trend of bright  $C_p$  asteroids in other families shown in table 6 is similar to the spectral trend for all bright  $C_p$  asteroids. This might be caused by common process, not by common composition; one of the candidates of the common process is thermal metamorphism due to frequently impact events. Carbonaceous chondrites are known to get brighter albedo values upon thermal metamorphism (Hiroi et al. 1993; Cloutis et al. 2012). The area where the impact event raises the temperature to occur such a metamorphism is limited to several times as large as the size of the projectile at most (e.g., Davison et al. 2014; Kurosawa & Genda 2018). In addition, the area around the impact point becomes fine ejecta, impact metamorphosed asteroids may not remain as large objects. Thus the ratio of bright  $C_p$ -class asteroids in the family composed of low albedo asteroid members is considered to be small as a few percent (table 6).

The ratio of all bright  $C_p$ -complex asteroids in the total population is different from that in low albedo families. This might be caused by other factors than impact thermal metamorphism. Since DeMeo K-type and Xn-type asteroids were identified as spectral type of bright C-complex asteroids in this study, bright  $C_p$ -complex asteroids not belonging to any families are considered to be composed of CV/CK chondrites, enstatite chondrites/achondrites, or impact metamorphosed carbonaceous chondrites.

## 6 Conclusions

Spectroscopic observations of bright C-complex asteroids were carried out to unravel the origin and properties of asteroids. The results suggest that most bright C-complex (Bus) asteroids are composed of DeMeo C-type with concave curvature, B-type, Xn-type and K-type asteroids. The meteorites associated with these spectral asteroids have been found to be composed of minerals that have experienced high temperatures. Based on the comparison of observations in this study with the spectra of families, the origin of the bright C-complex asteroids can be

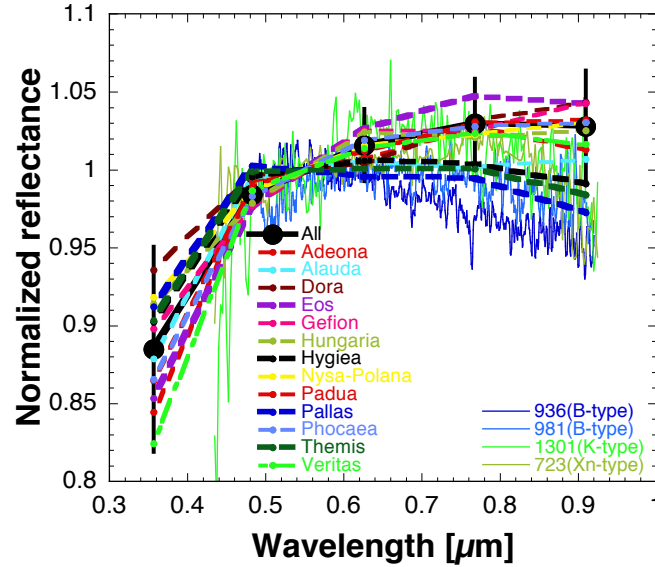


Fig. 5. Spectra for bright C-complex asteroids which are listed in this study and mean spectra of bright  $C_P$ -class asteroids belonging to each family.

Table 6. Proportion of bright C-complex asteroids in each family based on SDSS spectroscopic data in Carvano et al. (2010).

Family	All $C_P$ -comp*	Bright $C_P$ -comp*	Ratio of bright $C_P$ -comp	Albedo distribution <sup>†</sup>	Typical spectral type <sup>‡</sup>	Region
All	11714(780)	1509(25)	0.129			
Adeona	226(17)	4(0)	0.018	Low	Ch	Central main-belt
Dora	163(10)	3(0)	0.018	Low	Ch	Central main-belt
Hoffmeister	140(5)	0(0)	0.000	Low	C	Central main-belt
Padua	85(4)	3(1)	0.035	Low	X	Central main-belt
Hygiea	449(86)	27(2)	0.060	Low	C	Outer main-belt
Themis	550(160)	21(3)	0.038	Low	C	Outer main-belt
Veritas	175(1)	6(1)	0.034	Low	Ch	Outer main-belt
Alauda	199(25)	7(0)	0.035	Low	B,C,X	Outer main-belt, large $i$
Eos	241(0)	156(0)	0.647	Middle	K	Outer main-belt
Pallas	15(7)	10(6)	0.667	Middle	B	Central main-belt, large $i$
Nysa-Polana	283(41)	20(0)	0.071	Bimodal	F,S	Inner main-belt
Gefion	17(0)	2(0)	0.118	Bimodal	S,C	Central main-belt
Tirela	6(0)	0(0)	0.000	Bimodal	L,Ld	Outer main-belt
Phocaea	18(0)	4(0)	0.222	Bimodal	C,S	Inner main-belt, large $i$
Hungaria	5(0)	5(0)	1.000	High	Xe	Inside of main-belt, large $i$

\*Numbers in parentheses are the number of  $B_P$ -types in Alí-Lagoa et al. (2016) for which data are listed in Carvano et al. (2010).

<sup>†</sup>References for albedo distribution: Alauda family, Masiero et al. (2015); Phocaea family, Novaković et al. (2017); other, Masiero et al. (2011).

<sup>‡</sup>References for typical spectral type: Alauda family, Hsieh et al. (2018); Gefion family, Mothé-Diniz, Roig, & Carvano (2005); Nysa-Polana family, Cellino et al. (2001); Tirela family, Mothé-Diniz & Nesvorný (2008b); other, Masiero et al. (2015).

inferred as follows.

- The member of the Eos family, including the bright C-complex asteroids, are composed of CV/CK chondrite analogues.
- Salts may have been deposited in the Pallas, Themis and Hygiea parent bodies. It is likely that there was not much salts present in the parent body of the Themis and Hygiea family due to the paucity of bright C-complex asteroids in the families. On the contrary, it is possible that 2 Pallas had more salts than the Themis and Hygiea parent bodies

since the Pallas family composes more bright C-complex asteroids.

- For other families occupied by dark C-complex asteroids, the bright C-complex asteroids were most likely formed by impact thermal metamorphism.
- Bright C-complex asteroids that do not belong to any families could be linked with CV/CK chondrites and/or enstatite chondrites/achondrites, besides impact metamorphosed carbonaceous chondrites.

## Acknowledgments

We are grateful to Dr. Víctor M. Alf-Lagoa and Dr. Marcela I. Cañada Assandri for sharing valuable theirs SDSS photometric data. We would like to thank the referee for her/his careful reviewing and giving constructive suggestions, which helped us to improve the manuscript significantly. We are grateful to Dr. Masateru Ishiguro and Dr. Katsuhito Ohtsuka for insights and fruitful discussions. This study was based in part on data collected at Okayama Astrophysical Observatory and using the Subaru Telescope, which is operated by NAOJ. Data collected at Okayama Astrophysical Observatory are used, as well as data obtained from SMOKA, which is operated by the Astronomy Data Center, NAOJ. Taxonomic type results presented in this work were determined, in whole or in part, using a Bus–DeMeo Taxonomy Classification Web tool by Dr. Stephen. M. Slivan, developed at MIT with the support of National Science Foundation Grant 0506716 and NASA Grant NAG5-12355. This study has utilized the SIMBAD database, operated at CDS, Strasbourg, France and the JPL Small-Body Database Browser, operated at JPL, Pasadena, USA. We would like to express our gratitude to the staff members of Okayama Astrophysical Observatory and the Subaru Telescope for their assistance. DK is supported by Optical & Near-Infrared Astronomy Inter-University Cooperation Program, the MEXT of Japan. This study was supported by JSPS KAKENHI (grant nos. JP15K05277, JP17K05636, JP18K03723, JP19H00719, JP19H00725, JP20H00188, and JP20K04055) and by the Hypervelocity Impact Facility (former facility name: the Space Plasma Laboratory), ISAS, JAXA.

## References

- Alf-Lagoa, V., et al. 2016, *A&A*, 591, A14
- Binzel, R. P., et al. 2019, *Icarus*, 324, 41
- Binzel, R. P., Harris, A. W., Bus, S. J., & Burbine, T. H. 2001, *Icarus*, 151, 139
- Binzel, R. P., Rivkin, A. S., Stuart, J. S., Harris, A. W., Bus, S. J., & Burbine, T. H. 2004, *Icarus*, 170, 259
- Baudrand, A., Bec-Borsenberger, A., & Borsenberger, J. 2004, *A&A*, 423, 381
- Baudrand, A., Bec-Borsenberger, A., Borsenberger, J., & Barucci, M. A. 2001, *A&A*, 375, 275
- Bus, S. J., & Binzel, R. P. 2002a, *Icarus*, 158, 101
- Bus, S. J., & Binzel, R. P. 2002b, *Icarus*, 158, 146
- Carvano, J. M., Hasselmann, P. H., Lazzaro, D., & Mothé-Diniz, T. 2010, *A&A*, 510, A43
- Carruba, V. 2013, *MNRAS*, 431, 3557
- Castillo-Rogez, J., Neveu, M., McSween, H. Y., Fu, R. R., Toplis, M. J., & Prettyman, T. 2018, *Meteorit. Planet. Sci.*, 53, 1820
- Castillo-Rogez, J. C., & Schmidt, B. E. 2010, *Geophys. Res. Lett.*, 37, L10202
- Cellino, A., Zappalà, V., Doressoundiram, A., Di Martino, M., Bendjoya, Ph., Dotto, E., & Migliorini, F. 2001, *Icarus*, 152, 225
- Chapman, C. R., Morrison, D., & Zellner, B. 1975, *Icarus*, 25, 104
- Clark, B. E., et al. 2010, *J. Geophys. Res.*, 115, E06005
- Clark, B. E., Ockert-Bell, M. E., Cloutis, E. A., Nesvorný, D., Mothé-Diniz, T., & Bus, S. J. 2009, *Icarus*, 202, 119
- Davies, J. K., Harris, A. W., Rivkin, A. S., Wolters, S. D., Green, S. F., McBride, N., Mann, R. K., & Kerr, T. H. 2007, *Icarus*, 186, 111
- Davison, T. M., Ciesla, F. J., Collins, G. S., & Elbeshhausen, D. 2014, *Meteorit. Planet. Sci.*, 49, 2252
- DeMeo, F. E., Binzel, R. P., & Lockhart, M. 2014, *Icarus*, 227, 112
- DeMeo, F. E., Binzel, R. P., Slivan, S., M., & Bus, S. J. 2009, *Icarus*, 202, 160
- Doressoundiram, A., Barucci, M. A., Fulchignoni, M., Florczak, M. 1998, *Icarus*, 131, 15
- Duffard, R., & Roig, F. 2009, *Planet. Space Sci.*, 57, 229
- de León, J., Pinilla-Alonso, N., Campins, H., Licandro, J., & Marzo, G. A. 2012, *Icarus*, 218, 196
- De Sanctis, M. C., et al. 2016, *Nature*, 536, 54
- Drilling, J. S., & Landolt, A. U. 1979, *AJ*, 84, 783
- Cloutis, E. A., Hudon, P., Hiroi, T., Gaffey, M. J., & Mann, P. 2012, *Icarus*, 221, 984
- Fornasier, S., Lantz, C., Barucci, M. A., & Lazzarin, M. 2014, *Icarus*, 233, 163
- Grav, T., et al. 2011, *ApJ*, 742, 40
- Grav, T., et al. 2012, *ApJ*, 744, 197
- Greenwood, R. C., Franchi, I. A., Kearsley, A. T., & Alard, O. 2010, *Geochim. Cosmochim. Acta*, 74, 1684
- Hasegawa, S., et al. 2014, *PASJ*, 66, 89
- Hasegawa, S., et al. 2018, *PASJ*, 70, 114
- Hasegawa, S., Hiroi, T., Ohtsuka, K., Ishiguro, M., Kuroda, D., Ito, T., & Sasaki, S. 2019, *PASJ*, 71, 103
- Hasegawa, S., Kuroda, D., Yanagisawa, K., & Usui, F. 2017, *PASJ*, 69, 99
- Hasegawa, S., Müller, T. G., Kuroda, D., Takita, S., & Usui, F. 2013, *PASJ*, 65, 34
- Hiroi, T., Pieters, C. M., Zolensky, M. E., & Lipschutz, M. E. 1993, *Science*, 261, 1016
- Hiroi, T., Zolensky, M. E., Pieters, C. M., & Lipschutz, M. E. 1996, *Meteorit. Planet. Sci.*, 31, 321
- Hsieh, H. H., Novaković, B., Kim, Y., & Brasser, R. 2018, *AJ*, 155, 96
- Ishigaki, T., et al. 2004, *PASJ*, 56, 723
- Iwai, A., Itoh, Y., Terai, T., Gupta, R., Sen, A., & Takahashi, J. 2017, *Res. Astron. Astrophys.*, 17, 17
- Johnson, T. V., & Fanale, F. P. 1973, *J. Geophys. Res.*, 78, 8507
- Kasuga, T., Usui, F., Ootsubo, T., Hasegawa, S., & Kuroda, D. 2013, *AJ*, 146, 1
- Kasuga, T., Usui, F., Shirahata, M., Kuroda, D., Ootsubo, T., Okamura, N., & Hasegawa, S. 2015, *AJ*, 149, 37
- Keil, K. 1989, *Meteoritics*, 24, 195
- Keil, K. 2010, *Chem. Erde*, 70, 295
- Kobayashi, N., et al. 2000, in *SPIE Proc.*, 4008, Optical and IR Telescope Instrumentation and Detectors, ed. M. Iye & A. F. Moorwood (Bellingham: SPIE), 1056
- Kurosawa, K., & Genda, H. 2018, *Geophys. Res. Lett.*, 45, 620
- Lazzaro, D., Angeli, C. A., Carvano, J. M., Mothé-Diniz, T., Duffard, R.,

- & Florczak, M. 2004, *Icarus*, 172, 179
- Lazzarin, M., Marchi, S., Barucci, M. A.; Di Martino, M., & Barbieri, C. 2004a, *Icarus*, 169, 373
- Lazzarin, M., Marchi, S., Magrin, S., & Barbieri, C. 2004b, *Mem. S. A. It. Suppl.*, 5, 21
- Lazzarin, M., Marchi, S., Magrin, S., & Licandro, J. 2005, *MNRAS*, 359, 1575
- Lucas, M. P., et al. 2019, *Icarus*, 332, 227
- Mainzer, A. et al. 2011a, *ApJ*, 743, 156
- Mainzer, A., et al. 2011b, *ApJ*, 741, 90
- Mainzer, A., et al. 2012, *ApJ*, 745, 7
- Marchi, S., Lazzarin, M., Paolicchi, P., & Magrin, S. 2005, *Icarus*, 175, 170
- Marsset, M., et al. 2020, *Nat. Astron.*, 4, 569
- Marsset, M., Vernazza, P., Birlan, M., DeMeo, F., Binzel, R. P., Dumas, C., Milli, J., & Popescu, M. 2016, *A&A*, 586, A15
- Masiero, J. R., DeMeo, F. E., Kasuga, T., & Parker, A. H. 2015, in *Asteroids IV*, ed. P. Michel et al. (Tucson: Univ. of Arizona Press), 323
- Masiero, J. R., Wright, E. L., & Mainzer, A. K. 2019, *AJ*, 158, 97
- Masiero, J. R., et al. 2011, *ApJ*, 741, 68
- Masiero, J. R., et al. 2012, *ApJL*, 759, L8
- Masiero, J. R., Grav, T., Mainzer, A. K., Nugent, C. R., Bauer, J. M., Stevenson, R., & Sonnett, S. 2014, *ApJ*, 791, 121
- Marzari, F., Davis, D., & Vanzani, V. 1995, *Icarus*, 113, 168
- McCord, T., Adams, J., & Johnson, T. V. 1970, *Science*, 168, 1445
- McCord, T., & Gaffey, M. J. 1974, *Science*, 186, 352
- Minowa, Y., et al. 2010, in *SPIE Proc.*, 7736, *Adaptive Optics Systems II*, ed. B. L. Ellerbroek et al. (Bellingham: SPIE), 77363N
- Moskovitz, N. A., Jedicke, R., Gaidos, E., Willman, M., Nesvorný, D., Fevig, R., & Ivezić, Ž. 2008a, *Icarus*, 198, 77
- Moskovitz, N. A., Lawrence, S., Jedicke, R., Willman, M., Haghighipour, N., Bus, S. J., & Gaidos, E. 2008b, *ApJ*, 682, L57
- Mothé-Diniz, T., Carvano, J. M., Bus, S. J., Duffard, R., & Burbine, T. H. 2008, *Icarus*, 195, 277
- Mothé-Diniz, T., & Nesvorný, D. 2008a, *A&A*, 486, L9
- Mothé-Diniz, T., & Nesvorný, D. 2008b, *A&A*, 492, 593
- Mothé-Diniz, T., Roig, F., & Carvano, J. M. 2005, *Icarus*, 174, 54
- Murakami, H., et al. 2007, *PASJ*, 59, S369
- Novaković, B., Tsirvoulis, G., Granvik, M., & Todović, A. 2017, *AJ*, 153, 266
- Neeley, J. R., Clark, B. E., Ockert-Bell, M. E., Shepard, M. E., Conklin, J., Cloutis, E. A., Fornasier, S., & Bus, S. J. 2014, *Icarus*, 238, 37
- Ohtani, H., et al. 1998, in *SPIE Proc.*, 3355, *Optical Astronomical Instrumentation*, ed. S. D'Odorico, (Bellingham: SPIE), 750
- Ostrowski, D. R., Lacy, C. H. S., Gietzen, K. M., & Sears, D. W. G. 2011, *Icarus*, 212, 682
- Poch, O., et al. 2020, *Science*, 367, aaw7462
- Popescu, M., et al. 2016, *A&A*, 591, A115
- Rivkin, A. S., Binzel, R. P., Howell, E. S., Bus, S. J., & Grier, J. A. 2003, *Icarus*, 165, 349
- Roig, F., Nesvorný, D., Gil-Hutton, R., & Lazzaro, D. 2008, *Icarus*, 194, 125
- Sykes, M. V., Cutri, R., M., Fowler, J. W., Tholen, D. J., Skrutskie, M. F., Price, S., & Tedesco, E. F. 2000, *Icarus*, 146, 161
- Tedesco, E. F., Cellino, A., & Zappalà, V. 2005, *AJ*, 129, 2869
- Tedesco, E. F., Noah, R. V., Noah, M., & Price, S. D. 2002, *AJ*, 123, 1056
- Tedesco, E. F., Williams, J. G., Matson, D. L., Weeder, G. J., Gradie, J. C., & Lebofsky, L. A. 1989, *AJ*, 97, 580
- Tholen, D. J. 1984, PhD thesis, Arizona University
- Tokunaga, A. T., et al. 1998, in *SPIE Proc.*, 3354, *Infrared Astronomical Instrumentation*, ed. A. M. Fowler (Bellingham: SPIE), 512
- Usui, F., et al. 2011, *PASJ*, 63, 1117
- Usui, F., Hasegawa, S., Ootsubo, T., & Onaka, T. 2019, *PASJ*, 71, 1
- Usui, F., Kasuga, T., Hasegawa, S., Ishiguro, M., Kuroda, D., Müller, T. G., Ootsubo, T., & Matsuhara, H. 2013, *ApJ*, 762, 56
- Vernazza, P., et al. 2015, *ApJ*, 806, 204
- Vernazza, P., et al. 2016, *AJ*, 152, 54
- Vernazza, P., et al. 2020, *Nat. Astron.*, 4, 136
- Weisberg, M. K., McCoy, T. J., & Krot, A. N. 2006, in *Meteorites and the Early Solar System II*, ed. D. S. Lauretta and H. Y. McSweeney Jr. (Tucson: Univ. of Arizona Press), 19
- Wright, E. L., et al. 2010, *AJ*, 140, 1868
- Yang, B., Zhu, J., Gao, J., Ma, J., Zhou, X., Wu, H., & Guan, M. 2003, *AJ*, 126, 1086
- Yang, B., Lucey, P., & Glotch, T. 2013, *Icarus*, 223, 359
- Zellner, B., Tholen, D. J., & Tedesco, E. F. 1985, *Icarus*, 61, 355

